Zn2+ inhibits spatial memory and hippocampal place cell representation through high-affinity binding to the NMDA receptor GluN2A subunit

Joanna Sikora, Sonia Di Bisceglie Caballero, David Reiss, Brigitte Kieffer, Pierre Paoletti, Pierre-Yves Jacob, Abdel-Mouttalib Ouagazzal

iScience

CellPress
OPEN ACCESS

Article

Zn^{2+} inhibits spatial memory and hippocampal place cell representation through high-affinity binding to the NMDA receptor GluN2A subunit

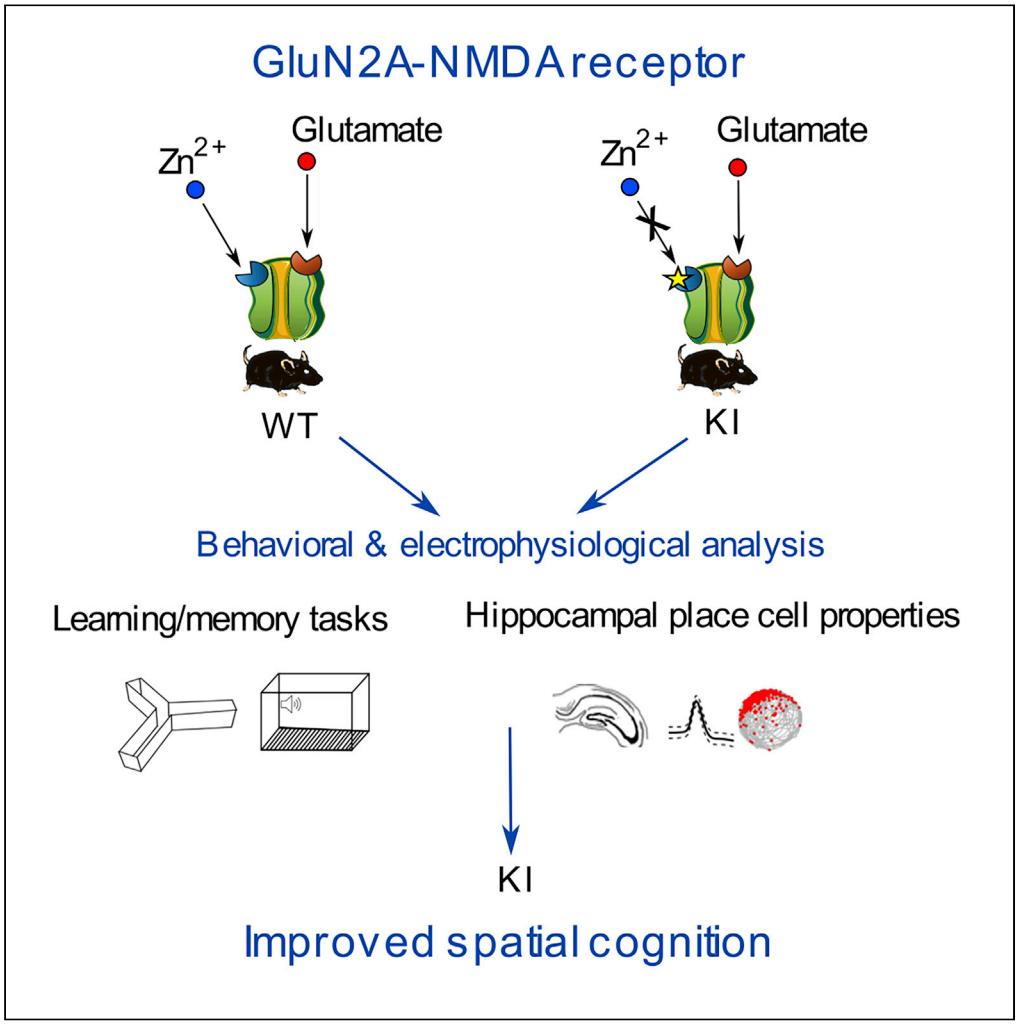

Joanna Sikora, Sonia Di Bisceglie Caballero, David Reiss, Brigitte L. Kieffer, Pierre Paoletti, Pierre-Yves Jacob, Abdel-Mouttalib Ouagazzal

abdel-mouttalib.ouagazzal@univ-amu.fr

Highlights

Zn^{2+} inhibits NMDA receptors via high-affinity binding site on the GluN2A subunit

Disruption of Zn^{2+}-GluN2A binding improves contextual fear learning in mice

Loss of Zn^{2+} action on GluN2A improves short-term spatial memory formation

Disruption of Zn^{2+}-GluN2A binding enhances hippocampal place cell representation

Sikora et al., iScience *25*, 105355
November 18, 2022
https://doi.org/10.1016/j.isci.2022.105355

iScience

CellPress
OPEN ACCESS

Article

Zn^{2+} inhibits spatial memory and hippocampal place cell representation through high-affinity binding to the NMDA receptor GluN2A subunit

Joanna Sikora,[1,2,6] Sonia Di Bisceglie Caballero,[1,2] David Reiss,[3] Brigitte L. Kieffer,[4] Pierre Paoletti,[5] Pierre-Yves Jacob,[1] and Abdel-Mouttalib Ouagazzal[1,7,*]

SUMMARY

A subset of glutamatergic neurons in the forebrain uses labile Zn^{2+} as a co-transmitter alongside glutamate. Synaptic Zn^{2+} plays a key role in learning and memory processes, but its mechanisms of action remain poorly understood. Here, we used a knock-in (KI) mouse line carrying a point mutation at the GluN2A Zn^{2+} binding site that selectively eliminates zinc inhibition of NMDA receptors. Ablation of Zn^{2+}-GluN2A binding improves spatial memory retention and contextual fear memory formation. Electrophysiological recording of hippocampal neurons in the CA1 area revealed a greater proportion of place cells and substantial place field remapping in KI mice compared to wildtype littermates. Persistent place cell remapping was also seen in KI mice upon repeated testing suggesting an enhanced ability to maintain a distinct representation across multiple overlapping experiences. Together, these findings reveal an original molecular mechanism through which synaptic Zn^{2+} negatively modulates spatial cognition by dampening GluN2A-containing NMDA receptor signaling.

INTRODUCTION

In the forebrain, a subset of glutamatergic neurons uses Zn^{2+} as a co-transmitter alongside glutamate (Frederickson et al., 2000; Paoletti et al., 2009; Sensi et al., 2011). Synaptically released Zn^{2+} acts as a neuronal messenger and participates in a variety of behavioral processes. One of the most established findings is its contribution to learning and memory processes subserved by the hippocampus and amygdala, limbic structures where synaptic Zn^{2+} is particularly abundant (Paoletti et al., 2009; Sindreu and Storm, 2011; Ceccom et al., 2014; McAllister and Dyck, 2017; Takeda and Tamano, 2017; Sikora and Ouagazzal, 2021). Electrophysiological studies in hippocampal and amygdala slices showed that vesicular Zn^{2+} acts as a potent modulator of synaptic plasticity, such as long-term potentiation (LTP) and long-term depression, which are considered key cellular mechanisms for information storage and memory formation (Kodirov et al., 2006; Sindreu and Storm, 2011; Pan et al., 2011; Sensi et al., 2011; Vergnano et al., 2014; McAllister and Dyck, 2017; Takeda and Tamano, 2017). Accordingly, vesicular Zn^{2+} depletion following the deletion of the vesicular zinc transporter-3 (ZnT3) gene in mice disrupts spatial memory, recognition memory, and associative fear memory (Lassalle et al., 2000; Daumas et al., 2004; Adlard et al., 2010; Martel et al., 2010; Takeda et al., 2010; Sindreu and Storm, 2011; Sindreu et al., 2011). Pharmacological chelation of synaptically released Zn^{2+} directly into the hippocampus or the amygdala also impairs long-term potentiation and learning and memory abilities in rats and mice (Lassalle et al., 2000; Takeda et al., 2010; Pan et al., 2011; Ceccom et al., 2014; Takeda and Tamano, 2017). Although the present studies show that synaptic Zn^{2+} is recruited during learning and facilitates mnemonic functions, its precise mechanisms of action remain poorly understood. Upon its release, Zn^{2+} can directly interact with a myriad of targets at extracellular and intracellular levels (Paoletti et al., 2009; Sindreu and Storm, 2011; Sensi et al., 2011; McAllister and Dyck, 2017) and exerts both inhibitory and facilitatory modulatory influences on learning and memory processes depending on the synaptic targets and their localizations, although the net effect is mainly promnesic. Studies conducted with membrane-permeable and membrane-impermeable zinc chelators in the hippocampus showed that promnesic effects of synaptic Zn^{2+} are in part mediated at the intracellular level (Sindreu and Storm, 2011; McAllister and Dyck, 2017; Takeda and Tamano, 2017). In the CA3 region, synaptic Zn^{2+} was suggested to promote memory formation by directly suppressing a mitogen-activated protein kinases (MAPK) tyrosine phosphatase in mossy

[1]Aix-Marseille University, CNRS, LNC (UMR 7291), 13331 Marseille, France

[2]Aix-marseille Université, Marseille, France

[3]IGBMC, ICS, 1 Rue Laurent Fries, BP 10142, 67404 Illkirch, France

[4]INSERM U1114, Université de Strasbourg, Strasbourg, France

[5]Institut de Biologie de l'Ecole Normale Supérieure (IBENS), CNRS, INSERM, Université PSL, Paris, France

[6]Present address: Université de Bordeaux, CNRS, Institut des Maladies Neurodégénératives, (UMR 5293), Bordeaux, France

[7]Lead contact

*Correspondence: abdel-mouttalib.ouagazzal@univ-amu.fr

https://doi.org/10.1016/j.isci.2022.105355

fiber terminals, which leads to an upregulation of the presynaptic extracellular signal-regulated kinases 1/2 activity that regulates transcriptional activities necessary for memory stabilization (Sindreu and Storm, 2011). *In vitro*, Zn^{2+} has been shown to interact with many neuronal ion channels and principal neurotransmitter transporters and receptors. For instance, exogenously applied Zn^{2+} inhibits the activity of glutamate, $GABA_A$, and cholinergic receptors that play a central role in cognition (Paoletti et al., 2009; McAllister and Dyck, 2017). Deciphering the exact contribution of these synaptic targets of Zn^{2+} remains however a major challenge owing to the lack of selective pharmacological tools.

In the present study, we used a genetic approach to examine whether synaptic Zn^{2+} modulation of mnemonic function involves NMDA receptor-dependent mechanisms. Native NMDA receptors (NMDARs) are heteromers composed of an obligatory GluN1 subunit and one or more of the four regulatory GluN2 subunits (GluN2A-GluN2D) that determine the functional properties of the NMDAR channel. The GluN2A subunit, which is widely expressed in the adult nervous system, confers to NMDARs an exquisite sensitivity for extracellular Zn^{2+} (Monyer et al., 1994). The GluN2A subunit harbors a high-affinity Zn^{2+} binding site in the N-terminal domain that mediates allosteric inhibition of GluN2A-containing NMDARs by nanomolar zinc concentrations (Paoletti et al., 2009; Paoletti, 2011). We introduced a point mutation (GluN2A-H128S) in the GluN2A subunit zinc-binding site that selectively eliminates high-affinity zinc inhibition of NMDARs in mice (Nozaki et al., 2011). We previously demonstrated in hippocampal slices preparation that the disruption of Zn^{2+} action on the GluN2A subunit enhances NMDAR-mediated currents and NMDAR-dependent LTP in CA1 and CA3 areas (Vergnano et al., 2014). The increase of NMDAR-mediated currents could only be revealed upon repetitive stimulations of mossy fibers or Schaffer collaterals suggesting that crosstalk between Zn^{2+} and NMDARs may particularly take place in physiologically relevant conditions, such as those involving synaptic plasticity and learning. Here, we studied the consequence of Zn^{2+}-GluN2A binding site ablation on learning and memory performances in a range of cognitive tasks (contextual and auditory-cued fear conditioning, spatial memory, and aversive instrumental learning). To get further insight into the impact of GluN2A-H128S mutation on information processing within the hippocampus, electrophysiological recording of place cell firing properties was performed in the CA1 region. Hippocampal place cells are pyramidal neurons that fire at a high frequency when an animal occupies a specific location in its environment, called a place field. The firing patterns exhibited by place cell ensembles are unique for each environment and are thought to correspond to an internal map that supports spatial navigation and episodic memory (Nakazawa et al., 2004; Moser et al., 2008). A bulk of pharmacological and genetic studies showed that NMDARs participate in various aspects of hippocampal place cell functions. Systemic pharmacological blockades of NMDARs abolish the long-term stability of newly formed place fields in the CA1 region (Kentros et al., 1998; Rowland et al., 2011). Furthermore, the knockdown of NMDARs selectively in CA1 pyramidal cells reduces the proportion of CA1 place cells and leads to less precise and stable place fields (Nakazawa et al., 2004; Cabral et al., 2014; Sheffield et al., 2017). The contribution of synaptic Zn^{2+} to the modulation of hippocampal place cell features has not been reported to the best of our knowledge.

RESULTS

Disruption of Zn^{2+}-GluN2A binding improves contextual fear learning

We first studied the impact of the GluN2A-H128S mutation on cued and contextual fear conditioning, two distinct forms of aversive associative learning that involve discrete unisensory information processing and spatial information processing, respectively (Fanselow, 2000; LeDoux, 2000; Rudy et al., 2004). Male GluN2A-H128S knock-in (KI) mice and wildtype (WT) littermates were submitted to a fear conditioning paradigm, in which an auditory cue paired with a footshock was presented twice after four minutes of familiarization with the testing chamber (Figure 1A). There was no difference between genotypes in baseline activity and freezing behavior during the familiarization period ($p > 0.05$ post-hoc Student's *t*-test, Figure 1B **and BC, respectively**). Following exposure to the tone-footshock pairings, both genotypes displayed a suppression of activity ($F_{3,54} = 46.88$, $p < 0.0001$, a main effect of conditioning, Figure 1B) and increased freezing behavior ($F_{1,18} = 105.6$, $p < 0.0001$, a main effect of conditioning, Figure 1C). Compared to WT, KI mice had a significantly lower activity score during the first and second post-footshock periods (PFS1 and PFS2, $p < 0.05$, post-hoc Student's *t*-test following a significant conditioning × genotype interaction, $F_{3,54} = 3.04$, $p < 0.05$, Figure 1B). Global freezing scores over the post-footshock periods were also higher for KI mice compared to WT littermates (PFS1+2, $p < 0.05$, post-hoc Student's *t*-test following a significant conditioning × genotype interaction,

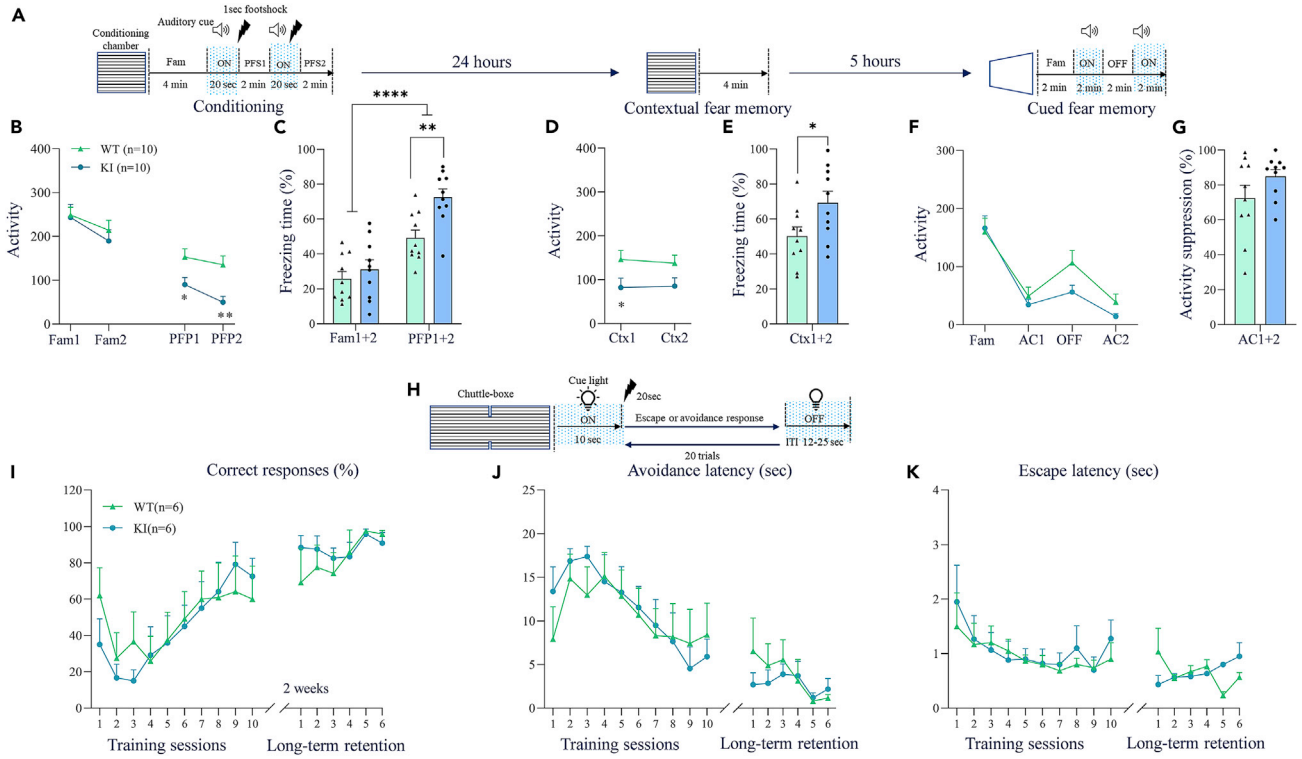

Figure 1. Conditioned fear learning and aversive instrumental learning performances of GluN2A-H128S knock-in (KI) mice and wildtype (WT) littermates

(A) Schematic diagram of the fear conditioning paradigm.

(B) Activity level per block of 2 min during the 4 min period of familiarization and after the presentation of the first and second footshock. Fam 1 and 2: first and second block of the familiarization period, respectively. PFS1 and 2: post-footshock periods 1 and 2, respectively.

(C) Time spent in freezing behavior (%) during the whole 4 min familiarization period (Fam1+2) and during the post-footshock period 1 and 2 pooled together (PFS1+2).

(D) Activity level per block of 2 min during the 4 min period of context testing. Ctx1 and 2: first and second blocks of the context testing period, respectively.

(E) Time spent in freezing behavior over the whole 4 min of context testing (Ctx1+2).

(F) Activity level per block of 2 min during familiarization (Fam) and after the auditory cue was turned ON (AC1 and AC2) and OFF.

(G) % of activity suppression during the presentation of the auditory cue relative to the familiarization period (AC1+2: 100*(mean of AC1 +AC2)/Fam). Auditory cue testing was carried out 5 h after context testing in a distinct chamber and different room.

(H) Schematic diagram of the two-way active avoidance paradigm.

(I and J) % correct responses and latency of correct avoidance responses respectively during the training sessions (20 trials per session once a day) and long-term retention testing (20 trials per session once a day) in the active-avoidance paradigm.

(K) Escape latency during shock presentation. Results are presented as mean ± SEM. *$p < 0.05$ and **$p < 0.01$ significantly different from WT mice, Student's *t*-test following a significant repeated measure ANOVA. ****$p < 0.0001$ significantly different from familiarization period, repeated measure ANOVA.

$F_{1,18} = 8.09$, $p = 0.01$, Figure 1C). Shock sensitivity assessed by motor reactions of mice to footshocks was comparable between genotypes (WT: 6.65 ± 0.38 and KI: 6.10 ± 0.41, $T_{18} = 0.98$, $p > 0.05$, Student's *t*-test), suggesting that the higher freezing level exhibited by KI mice reflect a rapid development of a conditioned fear response to the context and thus a better short-term contextual fear memory as previously demonstrated (Fanselow, 2000; Bast et al., 2003; Matus-Amat et al., 2004; Bannerman et al., 2008; Chang et al., 2008; Goeldner et al., 2009).

To assess long-term contextual fear memory retention, mice were re-exposed the following day to the conditioning chamber (Figure 1A). Both genotypes displayed contextual fear, but KI mice had again better scores than WT mice ($F_{1,8} = 5.05$, $p < 0.05$, the main effect of genotype Figure 1D and $T_{18} = 2.28$, $p < 0.05$, Student *t*-test, Figure 1E). Conditioned fear response to the auditory cue was then assessed 5 h later in different rooms and apparatuses used for conditioning (Figure 1A). No difference was detected between genotypes in any of the behavioral measures, but there was a trend toward an improvement (Figures 1F and 1G). A similar fear conditioning phenotype was revealed in female KI mice (Figures S1A–S1G) confirming that it is not gender-specific.

Disruption of Zn^{2+}-GluN2A binding unaffected fear-motivated instrumental learning

The lack of phenotype in auditory-cued fear conditioning raises the question of whether Zn^{2+} modulation of GluN2A-NMDARs may occur in more challenging aversive associative learning conditions. To test this, we used a two-way active avoidance paradigm, a fear-motivated instrumental task that requires incremental learning of goal-directed avoidance behavior (escape response) over multiple training trials (Figure 1H). In this task, mice learn to avoid a footshock by shuttling from one compartment to another during an auditory cue presentation. Both WT and KI mice acquired conditioned avoidance response to the auditory cue ($F_{15,\ 150} = 13.55$, $p < 0.0001$, Figure 1I), and no difference was detected between genotypes ($F_{1,10} \leq 0.0067$, $p > 0.05$ for % correct responses and avoidance latencies, Figures 1I and 1J, respectively). The latency of the escape responses to the footshock, which reflects nociceptive responses of the animals, was also comparable between WT and KI mice ($F_{1,\ 10} = 0.0018$, $p > 0.05$, Figure 1K). Long-term retention of active avoidance response was then assessed 2 weeks after the last training trial, but again no difference was observed between genotypes ($p > 0.05$ for all behavioral measures, Figures 1I–1K).

Disruption of Zn^{2+}-GluN2A binding improves spatial recognition memory

To explore further the impact of the mutation on mnemonic function, we used a two-trial Y-maze spatial recognition memory task that exploits the innate preference of rodents for novelty and does not involve any aversive stimuli. During the acquisition trial, mice are exposed only to two arms of the Y maze (start and familiar arms) and in the recall trial, they are exposed to all arms of the maze and the ability to discriminate novel from the familiar arm is used as an index of spatial recognition memory (Figure 2A). There was no difference between genotypes in baseline locomotor activity ($T_9 = 0.63$, $p > 0.05$, Student's *t*-test, Figure 2B) and time spent in the familiar arm (Table S1) during the acquisition trial. When the recall trial was carried out 15 min later, WT and KI mice discriminated novel from familiar arm ($p < 0.05$ *vs.* chance level, one-sample Student's *t*-test, Figure 2C) and no difference was detected between genotypes ($T_9 = 0.36$, $p > 0.05$). We next tested a longer retention delay (1 h) with the second batch of mice. Both genotypes had comparable locomotor activity during the acquisition ($T_{11} = 1.17$, $p > 0.05$, Student's *t*-test, Figure 2D), but KI mice spent a shorter time in the familiar arm (Table S1). In the recall trial, WT mice failed to discriminate novel from familiar arm ($p > 0.05$ *vs* chance level, one-sample Student's *t*-test, Figure 2E), demonstrating a delay-dependent forgetting. In contrast, KI mice had a good discrimination score ($p < 0.05$ *vs.* chance level, one-sample Student's *t*-test), and a significant improvement was detected compared to WT mice ($T_{11} = 2.48$, $p < 0.05$, Student's *t*-test, Figure 2E).

Disruption of the Zn^{2+}-GluN2A binding site improves hippocampal place cell representation

The above findings show that loss of Zn^{2+}-GluN2A biding site improves learning performances in cognitive tasks imposing spatial processing that has been shown to heavily depend on the hippocampus. We, therefore, examined whether the mutation impacts hippocampal place cell firing properties, which are thought to encode spatial memory representations (Hartley et al., 2014; Moser et al., 2017). We recorded CA1 hippocampal neurons, in WT and KI mice (1 female and 2 males for each genotype) that freely explore a circular arena polarized by a visual cue. First, we found a larger proportion of hippocampal neurons that are active in KI mice ($n = 316$) compared to WT mice ($n = 207$). This result was not attributed to the high baseline exploration level of KI mice as no difference was found between genotypes for distance traveled (WT: 33.5 $\pm$ 1.8 meters and KI: 38.6 $\pm$ 2.3 meters, *n.s.*, Student's *t*-test) and average locomotion speed (WT: 6.02 $\pm$ 0.27 cm/sec and KI: 6.98 $\pm$ 0.52 cm/sec, *n.s.*, Student's *t*-test, Table 1). In the total of recorded neurons, KI mice had an increased proportion of place cells ($X^2 = 29.949$, $p < 0.001$) among which a greater proportion shows theta modulation ($X^2 = 5.2026$, $p = 0.0226$) with higher intrinsic theta frequency ($p < 0.005$, Student's *t*-test, Table 1 and Figures 2F–2H). The spatial coherence of KI mice place cells was greater than WT mice indicating a better quality of the hippocampal spatial representation. Moreover, we observed increased spike height ($p < 0.005$, Student's *t*-test) and peak-to-trough duration ($p < 0.05$, Student's *t*-test) for KI mice place cells (Table 1). Other quantitative and qualitative parameters of place cells (Infield mean rate, infield peak rate, intrinsic theta power, spatial information content (IC), field size, and within-session stability, Table 1) were comparable between genotypes. Because KI place cells are more numerous and show greater theta modulation, we compared theta phase precession of place cells between KI and WT mice. The coupling of place cell theta-modulation action potentials with hippocampal theta local field potential oscillations, known as the phase precession process, is thought to provide a temporal code of the animal's ongoing path at the behavioral timescale (Climer et al., 2013; Moser et al., 2017). Both frequency and power of theta local field potential were comparable between groups (LFP theta frequency: WT: 7.9 $\pm$ 0.08 Hz and KI: 8.1 $\pm$ 0.06 Hz, *n.s.*, Student's *t*-test; LFP theta power; WT: 11.4 $\pm$ 1.6 and KI: 12.2 $\pm$ 1.4, *n.s.*,

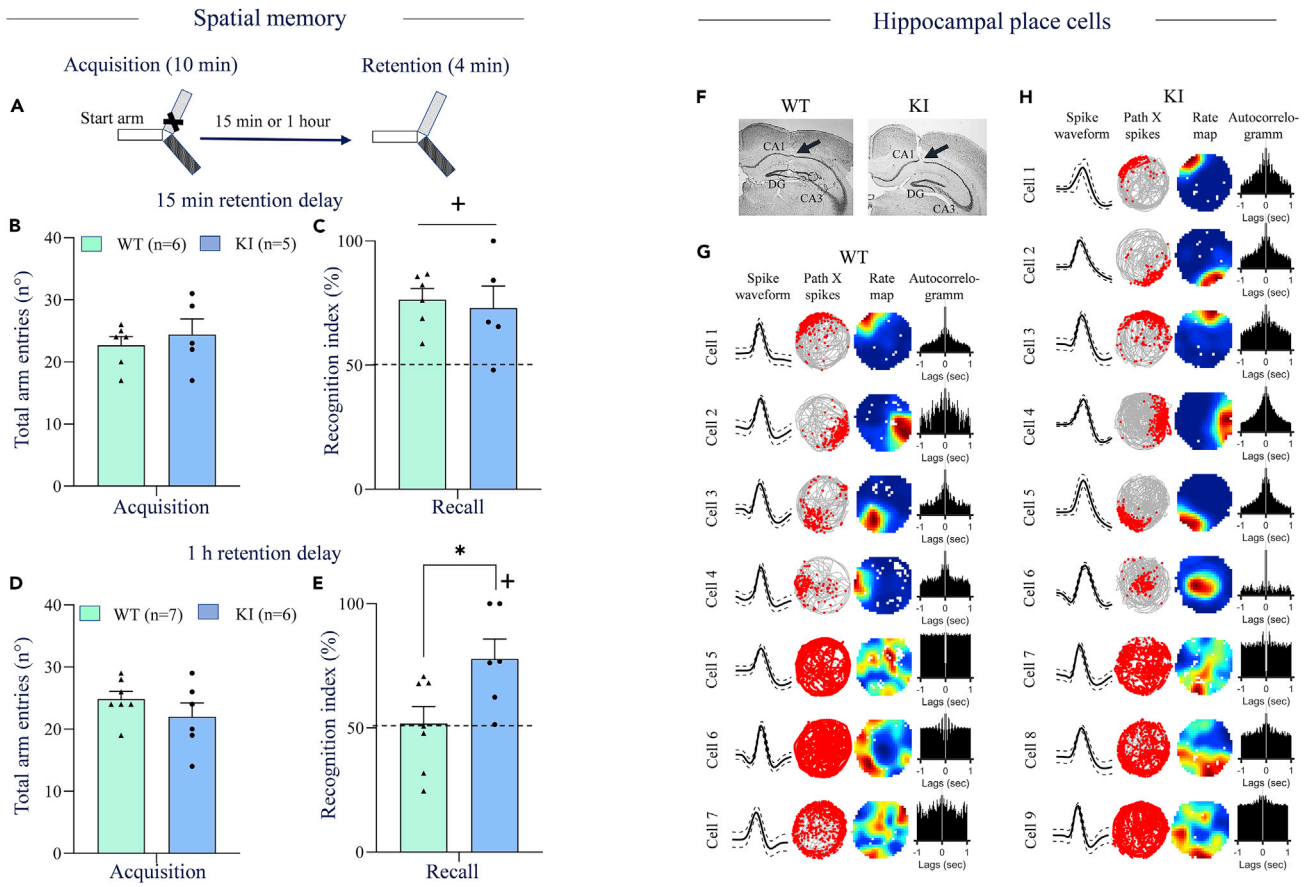

Figure 2. Spatial recognition memory performances and hippocampal CA1 place cell properties of GluN2A-H128S knock-in (KI) mice and wildtype (WT) littermates

(A) Schematic diagram of the Y-maze spatial recognition memory task.

(B) A total number of arm entries during the acquisition session (10 min) in a y-maze apparatus and C) Recognition memory performances after 15 min retention delay.

(D) A total number of arm entries during the acquisition (10 min) and E) Recognition memory performances after 1h retention delay. % recognition index is expressed as the ratio of preference for the novel arm over the familiar arm of the maze. The dashed line indicates the chance level.

(F) Coronal slices showing the position of electrodes for place cell recordings in the hippocampal CA1 region (black arrow) for WT (left) and KI (right) mice.

(G and H) CA1 place cell and non-place cell examples for WT (G) and KI (H) mice showing cell waveforms (left column), animal path (grey line) with spike superimposed (red dots) (middle-left), rate maps coded according to a color scale that goes from blue (0Hz) to red (maximum rate), with cyan, yellow and orange as intermediate firing from low to high (middle-right), and autocorrelograms of the firing activity in 1-s lags (right). Results are presented as mean ± SEM. *p < 0.05, significantly different from WT mice, Student's *t*-test. $^{+}$p < 0.05, significantly different from chance level, one group Student's *t*-test.

Student's *t*-test, Figures S2A–S2C). There was also no difference between genotypes in the proportion of place cells showing theta phase precession (WT: 21% and KI: 22%, $X^2 = 0.0296$, *n.s*, Figures S2D and S2E), as well as the slope of the theta phase precession (WT: −0.16 ± 0.07 and KI: −0.13 ± 0.02 Hz, *n.s.*, Student's *t*-test, Figure S2F).

Disruption of the Zn^{2+}-GluN2A binding site improves spatial discrimination

Following each delay exposure to the circular arena, mice underwent a sequence of testing (Figure 3A) to assess place cells cue control (circular arena randomly rotated), spatial remapping (exposure to an arena of distinct geometry) then place cell stability (re-exposure to the circular arena in the initial position). We calculated the difference between the place cell firing field's angle rotation and the angle of rotation of the arena and found that both KI and WT mice place cells showed a good cue control (Circular V-test for 0° mean angle, KI: v = 52.1070, p < 0.001, WT: v = 1.5129, p < 0.001; KI spatial correlation for KI = 0.77 ± 0.02 and WT = 0.72 ± 0.03, *n.s.*, Student's *t*-test on *Z* score, Figures 3B and 3C). Place cells also show a good place filed stability (spatial correlation for KI = 0.48 ± 0.02 and WT = 0.46 ± 0.05, *n.s.*, Student's *t*-test on *Z* score, Figures 3D

Table 1. Summary of behavior and cell distribution for WT and KI mice and main electrophysiological and spatial characteristics of CA1 place cells

	WT (n = 3)	KI (n = 3)
Behaviour		
Total distance (m)	33.5 ± 1.8	38.6 ± 2.3
Mean speed (cm/s)	6.02 ± 0.27	6.98 ± 0.52
Cell counts		
Number of recording sessions	27	26
Number of cells	207	316
Number of place cells	52	155
Proportion of place cells (%)	**25**	**49** ψ
Waveform characteristics		
Spike Height (μV)	**286.5 ± 12.4**	**335.4 ± 44.6** ***
Peak-to-trough (μs)	**337 ± 19.3**	**384 ± 9.3** *
Firing characteristics		
Overal (Hz)	1.03 ± 0.2	1.25 ± 0.11
Infield mean rate (Hz)	3.98 ± 0.54	4.47 ± 0.28
Infield peak Rate (Hz)	15.73 ± 1.89	15.95 ± 0.98
Intrinsic theta frequency (Hz)	**7.29 ± 0.13**	**7.70 ± 0.07** ***
Intrinsic theta power	3.78 ± 0.83	5.02 ± 0.63
Thêta modulation (%)	**65**	**87** ψ
Spatial characteristics		
Spatial coherence	**0.36 ± 0.02**	**0.44 ± 0.01** ***
IC (bits/spike)	1.44 ± 0.04	1.44 ± 0.04
Field size (cm^2)	275.6 ± 16.5	309.3 ± 10.3
Within-session stability	0.67 ± 0.03	0.69 ± 0.02

IC: Information content.
Averages are given ± SEM. Student's t-test: *, $p < 0.05$; ***, $p < 0.005$. χ^2: $\psi < 0.001$.

and 3E). For both place cell cue control and place cell stability, there was no difference between genotypes. We then examined whether transfer from a circular to a square arena that shares common perceptual features (Figure 3A) can induce a reorganization of place cell firing locations or spatial remapping, a process that reflects the creation of distinct hippocampal representation and thereby the ability of mice to discriminate overlapping spatial contexts (Muller and Kubie, 1987; Colgin et al., 2008). We used a square arena with a distinct color of walls (black *vs* light grey for the circular arena), but a similar color and texture of the floor. In both arenas, the visual cue was in the same position. For KI mice, we found that the spatial correlation of place cell activities between circular and square arenas was not different from 0 ($p < 0.005$, one-sample *t*-test) indicating place cell remapping across the two environments (Figures 3F and 3G). It was also significantly lower than the spatial correlation of WT mice ($p < 0.005$, Student's *t*-test, Figures 3F and 3G), suggesting a higher degree of remapping in KI mice. Accordingly, further analysis of the firing patterns (see STAR methods) showed that KI mice had a greater proportion of place cells (79%) that remapped in the square arena compared to WT littermates (44%, $X^2 = 21.9$, $p < 0.001$, Figures 3F and 3H).

Because the recording sequence was run over several days, we sought to determine whether remapping is modified with more exposure to the square arena. We found that spatial correlation between square and circular arenas progressively increased with repeated testing in WT mice indicating decreasing remapping but remained relatively constant over days with values close to 0 or below in KI mice (Figure 3I). The ANCOVA showed a group effect ($F_{1, 10} = 18.43$, $p < 0.001$), but no session effect and group × session interaction. Altogether, these results show a robust place cell remapping in KI mice that persist with repeated testing compared to WT mice, indicating an enhanced ability to process spatial information and maintain distinct representations across repeated overlapping experiences.

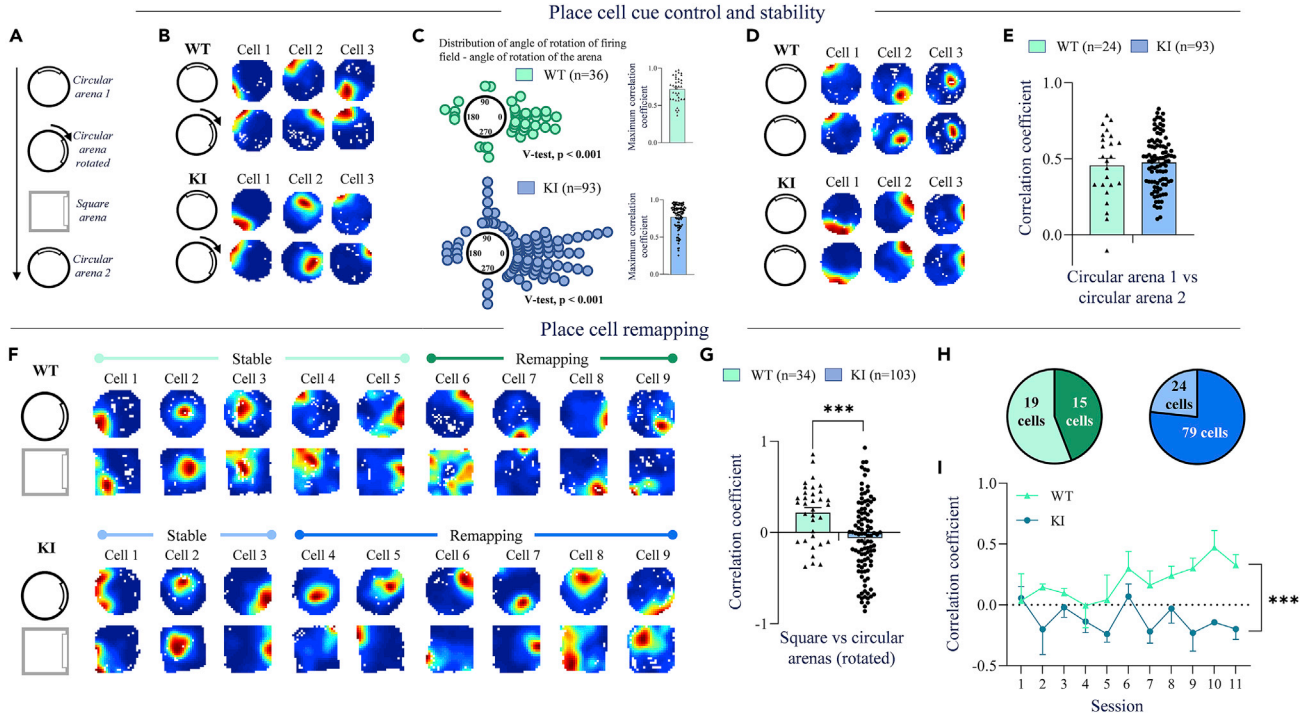

Figure 3. Hippocampal CA1 place cell cue control, stability, and remapping of GluN2A-H128S knock-in (KI) mice and wildtype (WT) littermates

(A) Protocol for place cells (PC) recording in a circular and a square arena.

(B) Examples of three PCs recorded in the circular arena (top – circular arena 1) and following 90° clockwise rotation of the arena (bottom - circular arena rotated). PCs show a firing field following the rotation, indicating a good control of PC spatial activity by the visual cue.

(C) Distribution of the differences in rotation angles between "circular arena 1" and "circular arena rotated" rate maps for which the spatial correlation is maximal. The circular V-test testing data distribution with a mean equal to 0° is significant for both groups (let). The average spatial correlation with individual values is shown for each group (right).

(D) Examples of three PCs recorded during the "circular arena 1" (top) and "circular arena 2" (bottom) sessions. PCs show good stability of spatial activity.

(E) Average spatial correlation of PC activity between the "circular arena 1" and "circular arena 2" sessions.

(F) Examples of nine PCs recorded in the circular arena (top) and the square arena (bottom). PC that does not change their spatial activity between arenas are labeled "Stable," while modified PC spatial activity is labeled "Remapping." KI mice display a larger number of remapping PC.

(G) Average spatial correlation of PC activity between the "circular arena rotated" and "square arena" sessions.

(H) Proportion of PCs showing remapping (dark color) or stable (light color) activity.

(I) Time course of average spatial correlation between circular and square arenas over recording sessions. KI mice show continuous PC remapping over sessions, while WT mice PCs become gradually stable between the two arenas. For C, E, and G, data from individual PCs are shown in black. Results are presented as mean ± SEM. ***$p < 0.001$ significantly different from WT mice, Student's *t*-test, or repeated measure ANCOVA.

DISCUSSION

Genetic and pharmacological studies in rodents showed that synaptic Zn^{2+} in the hippocampus and amygdala facilitates learning and memory performances (Lassalle et al., 2000; Takeda et al., 2010; Pan et al., 2011; Ceccom et al., 2014; Takeda and Tamano, 2017). The beneficial effects of Zn^{2+} were in part linked to its translocation into post-synaptic neurons and modulation of intracellular signaling pathways (Sindreu and Storm, 2011; McAllister and Dyck, 2017; Takeda and Tamano, 2017). Here, we reveal an original molecular mechanism through which synaptic Zn^{2+} negatively modulates spatial cognition by inhibiting GluN2A-NMDAR signaling. We show that mice lacking a high-affinity Zn^{2+} binding site at the GluN2A subunit display improved spatial cognition and hippocampal place-field representation.

In the fear conditioning paradigm, KI mice displayed improved acquisition and long-term retention of contextual fear memory compared to WT littermates. The cognitive phenotype cannot be attributed to changes in shock sensitivity. In both fear conditioning and active avoidance paradigms, the nociceptive reaction to footshocks was comparable between genotypes. The lack of phenotype in auditory-cued fear conditioning and the absence of fear generalization across testing contexts also argues against changes in shock sensitivity and indicates that GluN2A-H128S mutation has more impact on aspects of conditioned

fear learning that involve spatial information processing. The good spatial memory retention exhibited by KI mice in the Y-maze task provides further evidence that loss of Zn^{2+} inhibition of GluN2A-NMDARs improves hippocampal-dependent memories. Increased GluN2A-NMDAR function in the hippocampus and associated cortical areas may promote efficient contextual fear learning and spatial memory formation by enhancing the ability of mice to process contextual information and elaborate an adequate conjunctive contextual representation. It may also enhance memory retention by promoting synaptic plasticity processes underlying information storage. Accordingly, in hippocampal preparation, we found that the ablation of the Zn^{2+}-GluN2A biding site enhances NMDAR-dependent LTP in CA1 and CA3 areas (12), which is considered a synaptic form of the encoding memory trace. Ca^{2+} signal generated through NMDAR activates several kinases, including the calcium-calmodulin kinase II (CaMKII), the extracellular signal-regulated kinase/mitogen-activated protein kinase (ERK/MAPK) pathway, and the protein kinase C that modulates the properties and trafficking of receptors (e.g., increase synaptic delivery of glutamatergic AMPA receptors) and initiate the transcriptional activities and protein synthesis necessary for the establishment of durable changes in synaptic strength and efficacy (Citri and Malenka, 2008; Franchini and Carrano, 2020). By directly dampening GluN2A-NMDAR activity, synaptically released Zn^{2+} can downregulate the activity of many signaling pathways and thereby negatively modulate synaptic plasticity and memory storage. Overall, the cognitive improvements revealed in KI mice extend previous studies showing that pharmacological and genetic manipulations disrupting GluN2A-NMDAR function are mainly effective in impairing short-term memory formation and rapid acquisition of spatial information (Bannerman et al., 2008; Franchini and Carrano, 2020).

Characterization of CA1 place cell firing properties of KI mice in standard and well-controlled conditions revealed interesting electrophysiological phenotypes. Compared to WT littermates, KI mice had 1) a larger proportion of place cells that show 2) a better spatial activity, and 3) a stronger and more persistent remapping over repeated transfer from circular to the square arena, which collectively points to enhanced hippocampal processing of spatial information. More specifically, we found a larger population of place cells in KI mice that display alterations of their spike properties (i.e., a greater spike height and longer peak-to-trough spike duration) and spatial firing characteristics suggesting an improvement of hippocampal place representation. These findings provide new evidence that NMDARs in the CA1 region participate in the formation of place fields (Sheffield et al., 2017). KI mice had also more place cells with a rhythmic firing in the theta band. The theta-modulation of place cells, coupled with hippocampal local field potential, may form the phase precession process and is thought to provide a temporal code of the animal's ongoing path at the behavioral timescale (O'Keefe, 1993). Compared to WTs, KI mice had overall the same proportion of theta phase processing place cells (22% vs 21% for WTs) with a similar theta phase precession slope. Although there is no difference in the phase precession process, a large number of theta-modulated place cells with a better spatial activity found in KI mice may result in a better capacity to represent spatial trajectories. The good spatial coherence of KI mice place cells may be attributed to better integration of the information from CA3 and entorhinal cortex inputs, which control place field firings (Nakazawa et al., 2004; Brun et al., 2008; Bittner et al., 2015; Sheffield et al., 2017). This may be linked to an increase in the strength and the efficacy of active synapses from CA3 and EC pathways, caused by the loss of synaptic Zn^{2+} inhibition of GluN2A-NMDARs. As demonstrated by numerous studies, NMDAR-mediated synaptic plasticity at CA1 synapses plays a fundamental role in the proper formation and stability of the place fields (Kentros et al., 1998; Nakazawa et al., 2004; Cobar et al., 2017) and our previous study in hippocampal slices preparation suggests that synaptic Zn^{2+} action on GluN2A-NMDAR may mostly take place in physiological conditions involving synaptic plasticity and learning (Vergnano et al., 2014). The enhanced ability of KI mice to distinctly code individual spatial locations provides strong evidence that the ablation of the Zn^{2+}-GluN2A binding site increases the processing of spatial information within the hippocampus. Such ameliorations in hippocampal function may likely contribute to their improved performance in cognitive tasks imposing processing in the spatial domain. Further studies involving the recording of hippocampal place cell activities in the Y-maze and the fear conditioning paradigms should help clarify the link between changes in hippocampal place cell firing properties and behavioral performances.

More robust remapping of place cells was also observed in KI mice upon transfer from the circular to the square arena. Remapping reflects the creation of distinct hippocampal spatial representations (Muller and Kubie, 1987; Muller, 1996) for different environments and suggests engagement of the pattern separation mechanism that is important for limiting interference between related memories and thereby mitigating forgetting of past overlapping experiences (Colgin et al., 2008). An interesting observation was the gradual

divergence of place cell remapping that emerges between genotypes through repeated testing. In KI mice, remapping persisted across sessions while in WT mice it progressively vanished indicating poorer discrimination or generalization between different arenas. The generalization displayed by WT mice may be attributed to the decline of the novelty of the square arena features (e.g., geometry, size, wall color) through repeated presentations. That these 2 arenas shared several features, in particular, the color of the floor which has been shown to exert a strong influence on place cell activity (Jeffery, 2007; Colgin et al., 2008), which may have facilitated this generalization process. The persistent remapping seen in KI mice points to an enhanced ability to maintain a distinct representation across repeated overlapping experiences, a process critical for episodic memory. Such mnemonic capacity may be explained by the fact that the disruption of Zn^{2+}-GluN2A binding not only enhances the processing and coding of contextual information but also increases the storage capacity of the hippocampal network. The fact that a higher number of active hippocampal CA1 neurons was found in KI than in WT mice also supports this hypothesis and suggests the recruitment of large local networks during spatial exploration. These findings complement those reported in previous pharmacological and genetic studies showing that NMDARs are necessary for spatial learning and proper formation and coordination of CA1 place fields (Kiyama et al., 1998; Nakazawa et al., 2004; Bannerman et al., 2008; Franchini and Carrano, 2020).

Overall, these studies shed new light on the mechanisms of the action of synaptic Zn^{2+}. They reveal an original molecular mechanism through which synaptic Zn^{2+} negatively modulates spatial memory formation by dampening GluN2A-NMDAR activity. A such mechanism of synaptic Zn^{2+} action may likely extend beyond spatial cognition. Synaptic $Zn2^{+}$ was implicated in many behavioral processes, including olfaction, audition, and emotional and motor behaviors that recruit NMDARs (Blakemore et al., 2013; Anderson et al., 2015; Patrick Wu and Dyck, 2018; Sikora and Ouagazzal, 2021). Collectively, these findings suggest that the dysregulation of Zn^{2+} GluN2A-NMDAR functional interaction may contribute to many psychiatric and neurological disorders. The identification of several pathogenic mutations in the Grin2A gene (Gao et al., 2017; Fernández-Marmiesse et al., 2018; Strehlow et al., 2019) that impact the sensitivity of the GluN2A subunit to Zn^{2+} (Serraz et al., 2016; Gao et al., 2017) strongly support the critical role of the crosstalk between NMDAR and Zn^{2+} in human health.

Limitations of the study

In this study, we showed that the genetic ablation of the high-affinity Zn^{2+} binding site at GluN2A-NMDRs improves learning abilities in cognitive tasks that depend on the integrity of the hippocampus. We confirmed that the mutation enhances spatial information processing and place representation in the hippocampus by recording place cell activities in the CA1 area, the primary output of the hippocampus that broadcasts information to the cortex and other regions. Because the GluN2A-H128S KI mouse line has not been extensively characterized we cannot completely exclude that developmental compensatory changes may contribute to the above phenotypes, although several observations argue against this possibility. Analysis of the expression of the main excitatory glutamate receptors (AMPA, GluN2A- and GluN2B-containing receptors) and the inhibitory glycine receptor (GlyRα1 subunit, another target of Zn^{2+}) as well as the abundance of synaptic Zn^{2+} in the hippocampus revealed no changes in KI mice compared to wildtype littermates (Nozaki et al., 2011). In the present study, we focused on the spatial properties of CA1 place cells, which depend heavily on excitatory inputs from the CA3 area and prefrontal cortex that are also enriched in synaptic Zn^{2+} and could therefore contribute to the observed cognitive and electrophysiological phenotypes. Further studies are needed to clarify how the loss of Zn^{2+} action on GluN2A-NMDRs impacts spatial information processing in Zn^{2+}-enriched regions within and outside the hippocampus.

STAR★METHODS

Detailed methods are provided in the online version of this paper and include the following:

- KEY RESOURCES TABLE
- RESOURCE AVAILABILITY
  - Lead contact
  - Materials availability
  - Data and code availability
- EXPERIMENTAL MODEL AND SUBJECT DETAILS
  - Animals
- METHOD DETAILS

SUPPLEMENTAL INFORMATION

Supplemental information can be found online at https://doi.org/10.1016/j.isci.2022.105355.

ACKNOWLEDGMENTS

This work was supported by the Centre National de la Recherche Scientifique (CNRS), Aix-Marseille University (AMU), and Institut National de la Santé et de la Recherche Médicale (INSERM). We thank the Association France Parkinson (AFP), the Fondation de France (FF) for financial support, and the European Research Council (ERC Advanced Grant #693021 to P.P.). J. Sikora was supported by the Fondation Universitaire A*MIDEX and the Association France Parkinson (AFP).

AUTHOR CONTRIBUTIONS

Conceptualization, AM.O. and PY.J.; methodology, AM.O., PY.J., J.S. and D.R..; investigation, J.S., D.R., and S.DBC.; writing – original draft, AM.O., PY.J.; funding acquisition, AM.O., P.P., and BL.K.; resources, AM.O., PY.J., P.P., and BL.K.; KY.M.; supervision, AM.O. and PY.J.

DECLARATION OF INTERESTS

The authors declare no competing interests.

INCLUSION AND DIVERSITY

We worked to ensure sex balance in the selection of non-human subjects.

Received: April 6, 2022
Revised: August 11, 2022
Accepted: October 11, 2022
Published: November 18, 2022

REFERENCES

Adlard, P., Jacqui, M.P., David, I.F., and Ashley, I.B. (2010). Cognitive loss in zinc transporter-3 knock-out mice: a phenocopy for the synaptic and memory deficits of alzheimer's Disease? J. Neurosci. *30*, 1631–1636. https://doi.org/10.1523/JNEUROSCI.5255-09.2010.

Anderson, C.T., Charles, T.A., Robert, J.R., Melissa, L.Z., Daniel, Y.Z., Ulf-Peter, A., Stephen, J.L., and Thanos, T. (2015). Modulation of extrasynaptic NMDA receptors by synaptic and tonic zinc. Proc. Natl. Acad. Sci. USA *112*, E2705–E2714. https://doi.org/10.1073/pnas.1503348112.

Bannerman, D.M., Niewoehner, B., Lyon, L., Romberg, C., Schmitt, W.B., Taylor, A., Sanderson, D.J., Cottam, J., Sprengel, R., Seeburg, P.H., et al. (2008). NMDA receptor subunit NR2A is required for rapidly acquired spatial working memory but not incremental spatial reference memory. J. Neurosci. *28*, 3623–3630. https://doi.org/10.1523/JNEUROSCI.3639-07.2008.

Bast, T., Zhang, W.N., and Feldon, J. (2003). Dorsal hippocampus and classical fear conditioning to tone and context in rats: effects of local NMDA-receptor blockade and stimulation. Hippocampus *13*, 657–675. https://doi.org/10.1002/hipo.10115.

Bittner, K.C., Grienberger, C., Vaidya, S.P., Milstein, A.D., Macklin, J.J., Suh, J., Tonegawa, S., and Magee, J.C. (2015). Conjunctive input processing drives feature selectivity in hippocampal CA1 neurons. Nat. Neurosci. *18*, 1133–1142. https://doi.org/10.1038/nn.4062.

Blakemore, L.J., Tomat, E., Lippard, S.J., and Trombley, P.Q. (2013). Zinc released from olfactory bulb glomeruli by patterned electrical stimulation of the olfactory nerve. Metallomics *5*, 208–213. https://doi.org/10.1039/c3mt20158a.

Brun, V.H., Leutgeb, S., Wu, H.Q., Schwarcz, R., Witter, M.P., Moser, E.I., and Moser, M.B. (2008). Impaired spatial representation in CA1 after lesion of direct input from entorhinal cortex. Neuron *57*, 290–302. https://doi.org/10.1016/j.neuron.2007.11.034.

Cabral, H.O., Fouquet, C., Rondi-Reig, L., Pennartz, C.M.A., and Battaglia, F.P. (2014). Single-trial properties of place cells in control and CA1 NMDA receptor subunit 1-KO mice. J. Neurosci. *34*, 15861–15869. https://doi.org/10.1523/JNEUROSCI.5320-13.2014.

Ceccom, J., Halley, H., Daumas, S., and Lassalle, J.M. (2014). A specific role for hippocampal mossy fiber's zinc in rapid storage of emotional memories. Learn. Mem. *21*, 287–297. https://doi.org/10.1101/lm.033472.113.

Chang, S.D., Chen, D.Y., and Liang, K.C. (2008). Infusion of lidocaine into the dorsal hippocampus before or after the shock training phase impaired conditioned freezing in a two-phase training task of contextual fear conditioning. Neurobiol. Learn. Mem. *89*, 95–105. https://doi.org/10.1016/j.nlm.2007.07.012.

Citri, A., and Malenka, R.C. (2008). Synaptic plasticity : multiple forms, functions, and mechanisms. Neuropsychopharmacology *33*, 18–41. https://doi.org/10.1038/sj.npp.1301559.

Climer, J.R., Newman, E.L., and Hasselmo, M.E. (2013). Phase coding by grid cells in unconstrained environments: two-dimensional phase precession. Eur. J. Neurosci. *38*, 2526–2541. https://doi.org/10.1111/ejn.12256.

Cobar, L.F., Yuan, L., and Tashiro, A. (2017). Place cells and long-term potentiation in the hippocampus. Neurobiol. Learn. Mem. *138*, 206–214. https://doi.org/10.1016/j.nlm.2016.10.010.

Colgin, L.L., Moser, E.I., and Moser, M.B. (2008). Understanding memory through hippocampal remapping. Trends Neurosci. *31*, 469–477. https://doi.org/10.1016/j.tins.2008.06.008.

Daumas, S., Halley, H., and Lassalle, J.-M. (2004). Disruption of hippocampal CA3 network: effects on episodic-like memory processing in C57BL/6J mice. Eur. J. Neurosci. *20*, 597–600. https://doi.org/10.1111/j.1460-9568.2004.03484.x.

Fanselow, M.S. (2000). Contextual fear, gestalt memories, and the hippocampus. Behav. Brain Res. *110*, 73–81. https://doi.org/10.1016/S0166-4328(99)00186-2.

Fernández-Marmiesse, A., Kusumoto, H., Rekarte, S., Roca, I., Zhang, J., Myers, S.J., Traynelis, S.F., Couce, M.L., Gutierrez-Solana, L., and Yuan, H. (2018). A novel missense mutation in GRIN2A causes a nonepileptic neurodevelopmental disorder. Mov. Disord. *33*, 992–999. https://doi.org/10.1002/mds.27315.

Franchini, L., Carrano, N., Di Luca, M., and Gardoni, F. (2020). Synaptic gluN2A-containing NMDA receptors: from physiology to pathological synaptic plasticity. Int. J. Mol. Sci. *21*, 1538. https://doi.org/10.3390/ijms21041538.

Frederickson, C.J., Suh, S.W., Silva, D., Frederickson, C.J., and Thompson, R.B. (2000). Importance of zinc in the central nervous system: the zinc-containing neuron. J. Nutr. *130* (5 SUPPL), 1471–1483. https://doi.org/10.1093/jn/130.5.1471s.

Gao, K., Tankovic, A., Zhang, Y., Kusumoto, H., Zhang, J., Chen, W., XiangWei, W., Shaulsky, G.H., Hu, C., Traynelis, S.F., et al. (2017). Adenovo loss-of-function GRIN2A mutation associated with childhood focal epilepsy and acquired epileptic aphasia. PLoS One *12*, e0170818–e0170820. https://doi.org/10.1371/journal.pone.0170818.

Goeldner, C., Reiss, D., Wichmann, J., Kieffer, B.L., and Ouagazzal, A.M. (2009). Activation of nociceptin opioid peptide (NOP) receptor impairs contextual fear learning in mice through glutamatergic mechanisms. Neurobiol. Learn. Mem. *91*, 393–401. https://doi.org/10.1016/j.nlm.2008.12.001.

Hartley, T., Lever, C., Burgess, N., and O'Keefe, J. (2014). Space in the brain: how the hippocampal formation supports spatial cognition. Philos. Trans. R. Soc. Lond. B Biol. Sci. *369*, 20120510. https://doi.org/10.1098/rstb.2012.0510.

Jeffery, K.J. (2007). Integration of the sensory inputs to place cells: what, where, why, and how? Hippocampus *17*, 775–785. https://doi.org/10.1002/hipo.20322.

Kentros, C., Hargreaves, E., Hawkins, R.D., Kandel, E.R., Shapiro, M., and Muller, R.V. (1998). Abolition of long-term stability of new hippocampal place cell maps by NMDA receptor blockade. Science (New York, N.Y.) *280*, 2121–2126. https://doi.org/10.1126/science.280.5372.2121.

Kiyama, Y., Manabe, T., Sakimura, K., Kawakami, F., Mori, H., and Mishina, M. (1998). Increased thresholds for long-term potentiation and contextual learning in mice lacking the NMDA-type glutamate receptor ε1 subunit. J. Neurosci. *18*, 6704–6712. https://doi.org/10.1523/jneurosci.18-17-06704.1998.

Kodirov, S.A., Takizawa, S., Joseph, J., Kandel, E.R., Shumyatsky, G.P., and Bolshakov, V.Y. (2006). Synaptically released zinc gates long-term potentiation in fear conditioning pathways. Proc. Natl. Acad. Sci. USA *103*, 15218–15223. https://doi.org/10.1073/pnas.0607131103.

Lassalle, J.M., Bataille, T., and Halley, H. (2000). Reversible inactivation of the hippocampal mossy fiber synapses in mice impairs spatial learning, but neither consolidation nor memory retrieval the Morris navigation task. Neurobiol. Learn. Mem. *73*, 243–257. https://doi.org/10.1006/nlme.1999.3931.

LeDoux, J.E. (2000). Emotion circuits in the brain. Annu. Rev. Neurosci. *23*, 155–184. https://doi.org/10.1146/annurev.neuro.23.1.155.

Martel, G., Hevi, C., Friebely, O., Baybutt, T., and Shumyatsky, G.P. (2010). Zinc transporter 3 is involved in learned fear and extinction, but not in innate fear. Learn. Mem. *17*, 582–590. https://doi.org/10.1101/lm.1962010.

Matus-Amat, P., Emily, A.H., Ruth, M.B., and Jerry, W.R. (2004). The role of the dorsal Hippocampus in the acquisation and retrieval of context memory representations. J. Neurosci. *24*, 2431–2439. https://doi.org/10.1523/JNEUROSCI.1598-03.2004.

McAllister, B.B., and Dyck, R.H. (2017). Zinc transporter 3 (ZnT3) and vesicular zinc in central nervous system function. Neurosci. Biobehav. Rev. *80*, 329–350. https://doi.org/10.1016/j.neubiorev.2017.06.006.

Monyer, H., Burnashev, N., Laurie, D.J., Sakmann, B., and Seeburg, P.H. (1994). Developmental and regional expression in the rat brain and functional properties of four NMDA receptors. Neuron *12*, 529–540.

Moser, E.I., Kropff, E., and Moser, M.-B. (2008). Place cells, grid cells, and the brain's spatial representation system. Annu. Rev. Neurosci. *31*, 69–89. https://doi.org/10.1146/annurev.neuro.31.061307.090723.

Moser, E.I., Moser, M.B., and McNaughton, B.L. (2017). Spatial representation in the hippocampal formation: a history. Nat. Neurosci. *20*, 1448–1464. https://doi.org/10.1038/nn.4653.

Muller, R. (1996). A quarter of a century of place cells. Neuron *17*, 813–822. https://doi.org/10.1016/S0896-6273(00)80214-7.

Muller, R.U., and Kubie, J.L. (1987). The effects of changes in the environment on the spatial firing of hippocampal complex-spike cells. J. Neurosci. *7*, 1951–1968. https://doi.org/10.1523/jneurosci.07-07-01951.1987.

Nakazawa, K., McHugh, T.J., Wilson, M.A., and Tonegawa, S. (2004). NMDA receptors, place cells and hippocampal spatial memory. Nat. Rev. Neurosci. *5*, 361–372. https://doi.org/10.1038/nrn1385.

Nozaki, C., Vergnano, A.M., Filliol, D., Ouagazzal, A.M., Le Goff, A., Carvalho, S., Reiss, D., Gaveriaux-Ruff, C., Neyton, J., Paoletti, P., and Kieffer, B.L. (2011). Zinc alleviates pain through high-affinity binding to the NMDA receptor NR2A subunit. Nat. Neurosci. *14*, 1017–1022. https://doi.org/10.1038/nn.2844.

O'Keefe, J. (1993). Hippocampus, theta, and spatial memory. Curr. Opin. Neurobiol. *3*, 917–924. https://doi.org/10.1016/0959-4388(93)90163-S.

Pan, E., Zhang, X.a., Huang, Z., Krezel, A., Zhao, M., Tinberg, C.E., Lippard, S.J., and McNamara, J.O. (2011). Vesicular zinc promotes presynaptic and inhibits postsynaptic long-term potentiation of mossy fiber-CA3 synapse. Neuron *71*, 1116–1126. https://doi.org/10.1016/j.neuron.2011.07.019.

Paoletti, P. (2011). Molecular basis of NMDA receptor functional diversity. Eur. J. Neurosci. *33*, 1351–1365. https://doi.org/10.1111/j.1460-9568.2011.07628.x.

Paoletti, P., Vergnano, A.M., Barbour, B., and Casado, M. (2009). Zinc at glutamatergic synapses. Neuroscience *158*, 126–136. https://doi.org/10.1016/j.neuroscience.2008.01.061.

Patrick Wu, H.-P., and Dyck, R.H. (2018). Signaling by synaptic zinc is required for whisker-mediated, fine texture discrimination. Neuroscience *369*, 242–247. https://doi.org/10.1016/j.neuroscience.2017.11.020.

Rowland, D.C., Yanovich, Y., and Kentros, C.G. (2011). A stable hippocampal representation of a space requires its direct experience. Proc. Natl. Acad. Sci. USA *108*, 14654–14658. https://doi.org/10.1073/pnas.1105445108.

Rudy, J.W., Huff, N.C., and Matus-Amat, P. (2004). Understanding contextual fear conditioning: insights from a two-process model. Neurosci. Biobehav. Rev. *28*, 675–685. https://doi.org/10.1016/j.neubiorev.2004.09.004.

Sensi, S.L., Paoletti, P., Koh, J.Y., Aizenman, E., Bush, A.I., and Hershfinkel, M. (2011). The neurophysiology and pathology of brain zinc. J. Neurosci. *31*, 16076–16085. https://doi.org/10.1523/JNEUROSCI.3454-11.2011.

Serraz, B., Grand, T., and Paoletti, P. (2016). Altered zinc sensitivity of NMDA receptors harboring clinically-relevant mutations. Neuropharmacology *109*, 196–204. https://doi.org/10.1016/j.neuropharm.2016.06.008.

Sheffield, M.E.J., Adoff, M.D., and Dombeck, D.A. (2017). Increased prevalence of calcium transients across the dendritic arbor during place field formation article increased prevalence of calcium transients across the dendritic arbor during place field formation. Neuron *96*, 490–504.e5. https://doi.org/10.1016/j.neuron.2017.09.029.

Sikora, J., and Ouagazzal, A.M. (2021). Synaptic zinc: an emerging player in Parkinson's Disease. Int. J. Mol. Sci. *22*, 4724. https://doi.org/10.3390/ijms22094724.

Sindreu, C., and Storm, D.R. (2011). Modulation of neuronal signal transduction and memory formation by synaptic zinc. Front. Behav. Neurosci. *5*, 68. https://doi.org/10.3389/fnbeh.2011.00068.

Sindreu, C., Palmiter, R.D., and Storm, D.R. (2011). Zinc transporter ZnT-3 regulates presynaptic Erk1/2 signaling and hippocampus-dependent

memory. Proc. Natl. Acad. Sci. USA *108*, 3366–3370. https://doi.org/10.1073/pnas.1019166108.

Strehlow, V., Heyne, H.O., Vlaskamp, D.R.M., Marwick, K.F.M., Rudolf, G., de Bellescize, J., Biskup, S., Brilstra, E.H., Brouwer, O.F., Callenbach, P.M.C., et al. (2019). GRIN2A -related disorders: genotype and functional consequence predict phenotype. Brain *142*, 80–92. https://doi.org/10.1093/brain/awy304.

Takeda, A., and Tamano, H. (2017). The impact of synaptic Zn2+ dynamics on cognition and its decline. Int. J. Mol. Sci. *18*, E2411. https://doi.org/10.3390/ijms18112411.

Takeda, A., Tamano, H., Imano, S., and Oku, N. (2010). Increases in extracellular zinc in the amygdala in acquisition and recall of fear experience and their roles in response to fear. Neuroscience *168*, 715–722. https://doi.org/10.1016/j.neuroscience.2010.04.017.

Vergnano, A.M., Rebola, N., Savtchenko, L.P., Pinheiro, P.S., Casado, M., Kieffer, B.L., Rusakov, D.A., Mulle, C., and Paoletti, P. (2014). Zinc dynamics and action at excitatory synapses. Neuron *82*, 1101–1114. https://doi.org/10.1016/j.neuron.2014.04.034.

STAR★METHODS

KEY RESOURCES TABLE

REAGENT or RESOURCE	SOURCE	IDENTIFIER
Chemicals, peptides, and recombinant proteins		
Cresyl violet	Sigma Aldrich, France	Cat# C5042
GELRED	Interchim, France	Cat#BY1740
Paraformaldehyde	Carl Roth, Germany	Cat# 4980.2
Isoflurane	Virbac, France	Cat# 200265
Experimental models: Organisms/strains		
GluN2A-H128S knock-in mice	Nozaki et al. (2011) and this paper	N/A
Oligonucleotides		
Primers for genotyping	Fisher Scientific, France	N/A
dNTPs	Carl Roth, Germany	Cat# 0178.1
Taq DNA Polymerase	Fisher Scientific, France	Cat# 11508626
Software and algorithms		
LabWatcher software	Viewpoint Life sciences, France	NA
Graphpad Prism 9	Graphpad software, CA, USA	N/A
Matlab R2022 with the following toolboxes: Signal Processing, Image Processing, Statistic and Machine Learning, Curve Fitting	Mathworks Inc., MathWorks, USA	9.12.0.1884302
DataWave Sciworks acquisition system	DataWave Technologies, Loveland, CO, USA	N/A
Offline sorter 2.8.8	Plexon Inc, Dalls, USA	N/A
Other		
8 tetrodes microdrives with MillMax connector	Axona Ltd, UK	N/A
Neuralynx amplifiers	Neuralynx, Bozeman, MT, USA	N/A
Fear conditioning chambers	Coulbourn Instruments, Allentown, US	The HABITEST modular behavioral test system
Shuttle-boxes	PanLa,b Barcelona, Spain	LE918
Recording circular and square arenas	Custom-made	N/A

RESOURCE AVAILABILITY

Lead contact

Further information and requests for resources and reagents should be directed to and will be fulfilled by the lead contact, Abdel-Mouttalib Ouagazzal (abdel-mouttalib.ouagazzal@univ-amu.fr).

Materials availability

This study did not generate new unique reagents.

Data and code availability

The data reported in this paper will be shared by the lead contact upon request.

This paper does not report original code.

Any additional information required to reanalyze the data reported in this paper is available from the lead contact upon request.

EXPERIMENTAL MODEL AND SUBJECT DETAILS

Animals

Adult wild-type (WT) and GluN2A-H128S knock-in (KI) male and female mice (14–19 weeks old, 28–32g) lacking the high-affinity zinc-binding site at the GluN2A subunit were used. A detailed description of the construction of this mouse line has been reported previously (Nozaki et al., 2011). Experimental cohorts were established by mating heterozygous males and females. They were maintained in 50% BL6JX129/SvPass genetic background. Mice were housed in groups of 3–4 in individually ventilated cages (Techniplast, Louviers, France) and kept in 12 h light/dark cycle (light on at 7:00, off at 19:00) with water and food ad-lib. Testing was performed during the light cycle between 9h00 and 17h00 at the Mouse Clinical Institute (ICS, Illkirch, France) and Laboratory of Cognitive Neurosciences (LNC, Marseille, France). All experimental procedures were conducted with the approval of the local French National Ethics Committees and in accordance with the EEC (2010/63/UE) guidelines for the care and use of laboratory animals.

METHOD DETAILS

Genotyping

Mice genotyping was performed by PCR analysis using the following primers and conditions. GluN2A-H128S primers: AGE5 (5′-AGCATCTGAGTACCCCATCTTCAAA-3′), AGH28 (5′-TCATCCCCATCTTGGGC ATTTCC-3′), AGH29 (5′-TCATCCCCATCTTGGGCATTCAT-3′) amplified for 45 cycles at 94°C for the 30s, 55°C for 30s and 72°C for 1min. PCRs were run in iCycler Thermal Cycler apparatus (Bio-Rad) products visualized after electrophoresis in 2.5% agarose gels with GelRed dye in E-BOX CX5.

Apparatus and behavioral procedures

Fear conditioning paradigm

Testing was conducted in operant chambers (Coulbourn Instruments, Allentown, US). The conditioning session was initiated with a 4 min habituation to the chamber followed by a 20-s presentation of a tone (conditional stimulus, SC) coupled at the last second with a footshock (0.4 mA). Two minutes later, a similar tone-shock pairing was presented, and mice were removed from the chamber 2 min later. An infra-red activity monitor (Coulbourn Instruments; Model H24-61MC; set to mouse sensitivity) that detects changes in the position of the animal's infrared body-heat signature (13 nM infrared radiation) in the x, y and z axes was used to assess the animal motion (sampling rate 100 ms). Activity level was analyzed over 2 min period. Freezing behavior was assessed by reanalyzing inactivity duration per 1 s (Graphic state Notation software 3.02, Coulbourn Instruments, see (Goeldner et al., 2009) for validation with visual scoring of freezing). Shock sensitivity was assessed by analyzing the motor reaction of mice over 2 s, starting at the presentation of the footshock. Contextual fear memory was assessed 24 h later by re-exposing mice to the conditioning chamber for 4 min. Cued fear memory was assessed 5 h later in five-choice operant chambers (Coulbourn Instruments, Allentown, United State) located in a different room. After a 2 min habituation to the new context, the tone was delivered for 2 min and this sequence was repeated once again. Basal fear response during familiarizations, immediate acquisition of conditioned fear during conditioning and fear memory retention were measured as changes in activity level and % time sent in freezing behavior. Cued fear memory was expressed as changes in activity level. Percentage of inactivity (ratio of activity suppression during the auditory cue presentation relative to familiarization period) during the presentation of the auditory cue was used as an index of learning because data from the Five-choice operant system could not be reanalyzed afterwards per blocks of 1 s owing to a computer issue.

Two-way active avoidance procedure

Training was conducted in four shuttle boxes (LE918, PanLab, Barcelona, Spain). Each trial began with the side currently occupied by the mouse being illuminated by a 10-s cue light (CS), which was used to signal a footshock (0.2 mA, 20-s duration) that was initiated by the offset of the CS. Mice never received the entire shock duration because they either escaped within 1–3 s to the other (unshocked) compartment or learned to avoid the footshock. A variable timeout period (range 15–25 s, no cue light) in which the mouse could freely explore the chamber was introduced between each trial. The training was conducted over 10 consecutive days (one session of 20 trials per day) for assessing acquisition performances and repeated two weeks later over 6 days to assess long-term memory retention. The numbers of avoidance responses (shuttle to the next compartment during the CS period) and escape during the shock presentation, the avoidance and escape latencies were recorded in each session. The correct avoidance responses (%) were expressed by the ratio (100 × (number of avoidance responses/total number of trials)).

Y-maze spatial recognition memory task

Testing was performed in a Y-shaped maze consisting of three white plexiglass arms (40 x 9 x16 cm) with white (start arm), and black and grey floor. Specific motifs were placed on the walls of each arm, thus allowing visual discrimination, and extra-maze cues of the room were also visible from the maze. The test consisted of acquisition and retention sessions separated by an inter-trial interval (ITI). In the acquisition trial, mice were placed at the end of the start arm and allowed to explore the maze for 10 min with one of the arms closed. They were then put back into their home cage located in a separate room. In the retention trial, mice were placed at the end of the start arm and allowed to explore freely all three arms of the maze for 4 min. The familiar and novel arms (blocked arm in the acquisition) were counterbalanced between genotypes. The time spent in familiar and novel arms was scored using LabWatcher software (Viewpoint Life sciences, France). The preference for a novel arm was used as an index of spatial recognition memory. The recognition index was expressed by the ratio (100× time spent in the novel arm)/(total time spent in familiar and novel arms)). A RI of 50% corresponds to a chance level, whereas a higher RI reflects a good spatial recognition memory.

Hippocampal place cell recording and data acquisition

Surgery and electrode implantation

Recordings were made using tetrodes, each composed of eight twisted 17 μm polyimide-coated platinum-iridium (90%/10%) wires (California Fine Wire, CA), attached to an Axona microdrive (Axona Ltd, Herts, UK). Mice were pre-treated subcutaneously with an analgesic (Buprenorphine 0.05 mg/kg) then under isoflurane anaesthesia (induction at 3–4% and maintained at 1–2%) the electrodes were chronically implanted in the left or right hippocampus (AP: +2, ML: ±2.1, DV: −1.3). Following surgery, all mice received subcutaneous injections of an anti-inflammatory (Rimadyl 5 mg/kg) and were allowed one week to recover. At the end of the experiment, mice were transcardially perfused with 4% paraformaldehyde (pentobarbital, Euthasol®, 800 mg/kg) and their brains were removed. Brains were frozen at −20°C and then sectioned every 40 μm, mounted and stained with cresyl violet to verify the final position of the electrodes.

Apparatus and recording setup

The first recording apparatus was a circular arena (50 cm diameter) with a 40 cm high wall. The walls and floor were covered with black and dark grey vinyl sheets respectively, allowing the experimenter to clean them between each recording. The second recording apparatus was a 50 cm × 50 cm square box with 40 cm high walls replacing the circular arena. The walls were covered with light grey vinyl sheets and the floor remains the same as the circular arena. Both arenas were polarized by a 30 cm wide x 40 cm high plastic white cue card attached to the wall. The apparatus was visually isolated from the rest of the room by a black cylindrical curtain (100 cm diameter) and lit by indirect light provided by four 25-W bulbs placed on the ceiling. A speaker was fixed to the ceiling in a central position relative to arenas, producing background noise >70 dB to mask uncontrolled directional sounds. The computer and recording set-up were located in a room adjacent to the room containing arenas.

Screening and recording were performed with a counterbalanced cable attached at one end to a commutator that allowed the mouse to move freely. The other end of the cable was connected to the mouse headstage, which contained a field-effect transistor amplifier for each wire. The signals from each tetrode wire were further amplified 10 000 times, bandpass-filtered between 0.3 and 3 kHz with Neuralynx amplifiers (Neuralynx, Bozeman, MT, USA), digitized (32 kHz), and stored by DataWave Sciworks acquisition system (DataWave Technologies, Loveland, CO, USA). One red light-emitting diode (LED) attached to the headstage assembly provided the position of the rat mouse. The LED was imaged with a CCD camera fixed to the ceiling above the arenas, and their position was tracked at 25 Hz with a digital spot-follower. Local field potentials (LFP) were recorded single-ended from one of the electrodes, simultaneously to single units. The signal was amplified 1000 times, lowpass-filtered at 500Hz, sampled at 1024Hz, and stored with the unit data.

Experimental procedure

We recorded place cells during a sequence of four 10–12 min recording sessions proceeded as follows:

Circular arena 1 - mice freely moved in the circular arena whose orientation relative to the outside room was random. Mice were placed in the arena, facing in a randomly determined direction.

Circular arena rotated - the circular arena was randomly rotated by 45° or 90° or 180°, clockwise or counter-clockwise, to check visual cue control of place cell activity.

Square arena - mice freely moved in the square arena.

Circular arena 2 - This session was run in the circular arena having the same orientation as in the session *circular arena 1*.

Between sessions, mice were removed from the apparatus and placed in a box in a random location outside the curtain for 2 min, in order to let the experimenter manipulates the arenas (rotation or change of the arena). The floor and walls of the arenas were cleaned between each session to neutralize olfactory cues. Mice were then mildly disoriented, by rotating their holding box, before the next session. Tetrodes were lowered 50 μm if no single-unit activity was found or after another a recording session.

Spike sorting

Spike sorting was performed manually using the graphical cluster-cutting software Offline Sorter (Plexon). Units selected for analysis had to have well-discriminated clusters with spiking activity clearly dissociated from background noise. Units that were lost, were not used for further analysis. Units having interspike intervals <2 ms (refractory period) were removed due to poor isolation, as were cells with a peak firing rate ≤1 Hz. We calculated the correlation value for clusters associated with a unit within each recording session. We set a correlation value threshold of 0.7, and cluster correlation above the threshold was used for further analysis. To prevent repeated recordings of the same cell over days, clusters that recurred on the same tetrodes in the same cluster space across recording sessions were only analyzed on the first day. A total of 438 cell clusters for KI mice and 252 cell clusters for WT mice were accepted.

Spatial rate maps

Spatial rate maps were generated by dividing the arena into an array of 40 × 40 cm square bins, each 2,5 × 2,5 cm in size. The number of spikes per bin was divided by the time spent in that bin to provide a firing rate (Hz). Smoothed firing rate maps were then generated using a boxcar procedure in which the firing rate in each bin was replaced by the mean rate of itself plus the immediately surrounding bins. The firing rate of the cell was colour-coded from low (light blue) to high (dark red). Pixels that were not visited by the rat were displayed in white.

Place cell selection

Cells were considered as place cells if a set of at least nine contiguous pixels had a firing rate above zero (i.e., place field) in *Circular arena 1*. Among the 690 cells, 52 for WT and 155 for KI groups were classified as place cells in *Circular arena 1*. Among them, 36 for WT and 94 for KI were recorded during *Circular arena rotated*, 34 for WT and 103 for KI were recorded during *Square arena* and 24 for WT and 93 for KI were recorded during *Circular arena 2*.

Waveforms

In the session *Circular arena 1*, we calculated the average spike waveform for each place cell. Then, we extracted the spike height (μV) as the difference between the maximum amplitude and the minimum amplitude of the waveform, and the peak-to-trough duration (μs) as the difference between the time at the maximum amplitude and the time at the minimum amplitude of the waveform. We compared waveform characteristics of the WT and KI groups using a non-paired Student's *t*-test.

Spatial firing analysis

To analyze the effects of ablation of Zn^{2+}-GluN2A biding on place cell firing properties, we calculated the field firing peak (Hz), the field size (cm^2), the spatial coherence and the spatial information for each place cell. Spatial coherence consists of spatial autocorrelation of the non-smoothed place field map and measures the extent to which the firing rate in a particular bin is predicted by the average rate of the eight surrounding bins. The spatial information content is expressed in bits per spike and is calculated as follows

$$I = \sum_i P_i\,(\lambda_i / \lambda) log_2(\lambda_i / \lambda)$$

Where λ_i is the mean firing rate in bin $_i$, λ is the overall mean firing rate and $_{Pi}$ is the occupancy probability of bin $_i$. In short, the spatial information content index can be seen as a measure of the amount of information relative to the location of the animal conveyed by a single action potential emitted by a single place cell. An X^2 test compares the proportion of place cells and a two-sample *t*-test compares spatial firing properties of place cells in *Circular arena 1* session between WT and KI groups.

Cue control

To analyze whether the place cell activity was controlled by the visual cue, for each cell we rotated the *circular arena rotated* rate map in steps of 6° and calculated the Pearson product-moment correlation coefficient between this rotated rate map and the *circular arena 1* rate map. We extracted the angle of rotation having the maximum correlation coefficient, which we subtracted to the angle of arena rotation. Thus, a value equal to 0° indicated that the place cell activity has followed the arena rotation. We have also compared the average correlation value between each group.

Stability

The stability of place cells activity was tested by calculating the correlation between *circular arena 1* and *circular arena 2* spatial rate maps.

Remapping

We performed two analyses to test whether place cell activity in circular and square arenas changed. First, for each cell, we calculated the correlation between the two rate maps constructed for the session in the square arena and the preceding session in the circular arena. Then, we compared the average correlation coefficient of KI mice with those of WT mice by a two-sample *t*-test as well as with the mean value equal to 0 by a one-sample *t*-test. Second, we run a shuffling procedure to classify whether place cells activity was stable or remaps. For each cell recorded in the square arena, we rotated the spike times with respect to the position vector by a random time drawn uniformly from the interval between 20 s and the recording duration minus 20 s. This procedure was repeated 400 times per cell. For each rotation, we reconstructed the spatial rate map, and we calculated the correlation with the circular arena rate map. We used the distribution of the correlation values from all rotations to set a statistical threshold at the ninety-fifth percentile of the distribution and we check whether the real correlation of circular *vs* square rate maps was under or above the threshold. A spatial correlation above the threshold indicates a stable place cell activity between the square and circular arena. Conversely, a spatial correlation under the threshold indicates that the place cell activity remaps between the square and circular arena. We observed that 51 cells were stable and 79 cells which remap for KI mice, 19 cells were stable and 15 which remap for WT mice.

Local field potentials and intrinsic firing analysis

In order to characterize the theta oscillations during the exploration of the arena, we applied a band-pass filter with cut-off frequencies in the theta band (4–12 Hz) and the delta band (2–4 Hz; 468 FMA Toolbox distributed under General Public License, http://fmatoolbox.sourceforge.net). We computed the Hilbert transform of the resulting oscillations and we calculated the instantaneous frequency from which we extracted the peak frequency in theta and delta bands. In order to compare the relative power of theta oscillations, we calculated the theta/(theta + delta) ratio by dividing the theta peak power by the sum of theta and delta peak powers. Finally, the intrinsic firing frequency of place cells in the theta band (4–12 Hz) was calculated by extracting the theta peak of the Hilbert transform of the cell spike autocorrelogram.

Phase precession

Two-dimensional phase precession of place cells was computed in the arena using the 'pass-index' Matlab function distributed under General Public License (https://github.com/jrclimer/Pass_Index) and developed by Climer et al. (2013). To compute the field index, we first calculated the occupancy-normalized firing rate for 1 cm square bins of position data. Data were then smoothed with a pseudo-Gaussian kernel with a five-pixel (5 cm) standard deviation. Each bin of the field index map was then attributed a value percentile normalized between 0 and 1. The omnidirectional pass index was computed on the raw rate maps. Quantification of phase precession was achieved by using the circular-linear correlation coefficient (rho) and the

statistical significance of the Pearson correlation (p value). A place cell was considered omnidirectionally precessing if the significance level of the correlation was below 0.05.

QUANTIFICATION AND STATISTICAL ANALYSIS

All behavioral data are expressed as mean group value ± standard error of the mean (SEM) and analyzed using unpaired Student's *t*-test or one-way ANOVA with repeated measures whenever it was appropriate. Unpaired Student's *t*-test was used when one-way ANOVA indicated a significant main effect of genotype or a significant interaction. One sample Student *t*-test was used to compare recognition index values to the chance level (50%). Electrophysiological properties were compared using an unpaired Student's *t*-test. X^2 was used to compare the proportion of PC between genotypes when appropriate. All Pearson's correlation coefficients had Fisher Z-transformation for statistical comparison. Circular statistics V-test was used to test cue control of place cells for each group. The criterion for statistical significance was $p < 0.05$.